

Title: Detonation Waves in PBX 9501

Author(s): RALPH MENIKOFF, *rtm@lanl.gov*

Submitted to: Combustion Theory and Modelling

Detonation Waves in PBX 9501

Ralph Menikoff[†]

Los Alamos National Laboratory

(January 2006)

For a planar detonation wave propagating in the plastic-bonded explosive PBX 9501, measurements of the reaction zone display a classical ZND profile. Moreover, the reaction-zone width is substantially less than the average size of an explosive grain. We show that the reaction zone is compatible with realistic constitutive properties and an Arrhenius reaction rate based on the bulk temperature. Thus, contrary to conventional wisdom, hot spots are not needed to propagate a detonation wave. Conventional wisdom is based, in part, on shock desensitization experiments; the observation that precompressing a PBX with a weak shock — which eliminates voids as nucleation sites for hot spots — can quench a propagating detonation wave. By analyzing the temperature behind two shocks compared to a single shock and the corresponding change of the induction time, we show that a detonation wave sustained by the bulk reaction rate from shock heating is compatible with shock desensitization. Shock desensitization depends on having a temperature sensitive rate, which usually is associated with detonation wave instability. However, for PBX 9501 the temperature variation in the reaction zone is small, and one-dimensional simulations show that this results in a stable detonation wave. Furthermore, we show that two additional phenomena are compatible with the perspective that bulk burn can sustain a planar detonation wave: failure diameter, which does depend on the heterogeneous structure of a PBX; and PBXs with a lower HE content which display an irregular detonation front.

AMS Subject Classification: 74J40; 74F25; 74E99; 76E30

Keywords: detonation wave; reaction zone; shock desensitization; wave stability; PBX 9501

1 Introduction

Initiation of a plastic-bonded explosive (PBX) requires hot spots. In addition, experiments have shown that a weak shock can desensitize a PBX and even quench a propagating detonation wave [1]. Conventional wisdom explains desensitization as due to compressing out voids and eliminating nucleation sites for hot spots. This appears to imply that hot spots are needed for propagation as well as initiation of a detonation wave. However, this is incompatible with measurements of the reaction zone profile described below.

Velocity interferometry techniques have reached the point that the reaction zone of a detonation wave can be fully resolved. Several experiments have been performed on HMX (cyclo-tetramethylenetetranitramine) based PBXs [2, 3, 4]. We focus on PBX 9501, which consists by weight of 95 % HMX, 2.5 % polyurethane binder and 2.5 % nitroplasticizer, pressed to within 1 to 2 % of its theoretical maximum density [see 5, pp. 109–119]. VISAR (Velocity Interferometry System for Any Reflector) measurements of the reaction zone of a planar Chapman-Jouguet (CJ) detonation wave displays a classical Zeldovich-von Neumann-Doering (ZND) profile; lead shock followed by smooth but rapid decrease in particle velocity. Moreover, the reaction-zone width is a fraction of the average grain size. In addition, PBX 9404 and EDC 37, which have similarly high HMX content but different binders,

[†]e-mail: rtm@lanl.gov

have nearly the same reaction zone profiles [2]. This suggests that the detonation wave is sustained by the bulk reaction from shock heating rather than hot spots. We show that the measured reaction zone is indeed compatible with realistic constitutive properties for HMX and an Arrhenius rate based on the bulk temperature.

The reaction zone analysis of a CJ detonation wave implies that eliminating hot-spot sites is necessary but not sufficient to explain shock desensitization. The quenching of a detonation wave as it propagates into a desensitized region can be viewed as an initiation problem. The bulk rate behind a shock at the CJ pressure is not sufficient for prompt initiation (sub μs time scale). However, the reaction zone of an impinging detonation wave provides a high pressure short duration pulse. By analyzing the temperature change due to two shocks compared to a single shock, along with the corresponding change of induction time, we show that a detonation wave sustained by the bulk reaction rate due to shock heating is compatible with shock desensitization.

We begin in sec. 2 by reviewing realistic constitutive properties that describe HMX. These include the equations of state (EOS) of the reactants and the products, and parameters for an Arrhenius reaction rate. For a temperature sensitive rate, the specific heat of the reactants is critically important. Since HMX is a large molecule ($\text{C}_4\text{H}_8\text{N}_8\text{O}_8$), it has many intra-molecular vibrational modes. Consequently, the specific heat is temperature dependent.

To compare a model with VISAR data for the reaction zone, one has to account for the impedance mismatch between the explosive and the VISAR window. Due to the nonlinearities of the problem, one-dimensional reactive-hydro simulations are used. The numerics are described in sec. 3. The simulated results for a planar CJ wave and comparison with experiments are presented in sec. 4.

Shock desensitization is discussed in sec. 5. A simulation is shown in which a detonation wave is quenched when it propagates into precompressed PBX 9501. This verifies that desensitization is compatible with a propagating detonation wave sustained by a bulk Arrhenius rate.

With a temperature sensitive rate, a propagating detonation wave is subject to a one-dimensional instability resulting in a pulsation known as a “galloping” detonation wave [see for example 6, chpt. 6A]. However, the effective temperature sensitivity is affected by the temperature variation within the reaction zone. The equation of state for PBX 9501 is such that the temperature at the von Neumann (VN) spike is only slightly less than the temperature at the CJ state. In this case, simulations presented in sec. 6 show that the detonation wave is stable.

Finally in sec. 7 we discuss two additional aspects of propagating detonation waves: (i) The front curvature of a detonation wave in a rate stick can lower the local detonation speed to the point at which the bulk reaction rate is not sufficient to propagate the wave. This leads to a change in reaction mode from bulk burn in the center, to hot spot dominated reaction at the edges. As a consequence, the failure diameter, which results from a rarefaction propagating inward from the edges, does depend on hot spots and hence the formulation of a PBX (grain distribution and binder). (ii) Similarly, other PBXs with a lower HMX content have a lower detonation speed, and the bulk reaction rate is not sufficient to propagate a detonation wave. Instead they have a reaction-zone width larger than the average grain size and the reaction rate is dominated by hot spots.

2 Constitutive properties

Detonation wave simulations require an EOS for the reactants and the products of the explosive, and a reaction model. At the high temperatures within the reaction zone, one decomposition mechanism is likely to dominate, and a single-step reaction (reactants to products) with an Arrhenius reaction is a reasonable model. Due to uncertainties in the available data, many constitutive models for PBX 9501 have been used. For just propagating a detonation wave, variations in the temperature from the specific heat or the shock Hugoniot can compensate for variations in the Arrhenius parameters to give a plausible reaction rate. Since we are interested in both the reaction zone for a propagating detonation wave and quenching when the wave propagates into a precompressed explosive, accurate constitutive properties are needed. Here the model we use is defined, along with the data on which it is based.

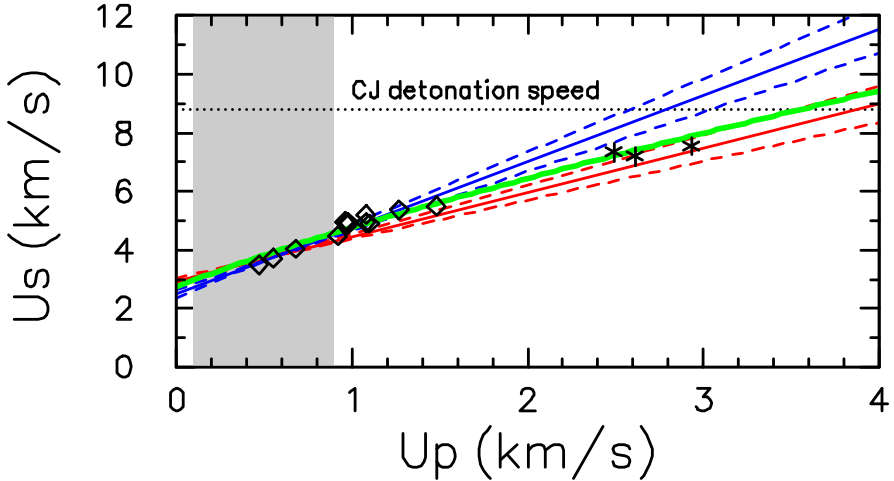


Figure 1. Unreacted Hugoniot for PBX 9501. Red and blue lines are from [5, §7.3, p. 116]; dashed lines are error bars and gray region is domain of fit. Green curve is fit to isothermal data [7, 8]. Black dotted line is CJ detonation speed (8.8 km/s). Diamonds are data points from [9] and stars are single crystal HMX data from [10, p. 595].

2.1 EOS of reactants

Data for the unreacted PBX 9501 Hugoniot and several fits in the (u_p, u_s) -plane are shown in fig. 1. The data up to $u_p = 1.5$ km/s (shock pressure of about 15 GPa) is compatible with several linear u_p - u_s fits in the literature [see for example 5, §7.3, p. 116]. Extrapolation to detonation velocity ($D=8.8$ km/s) gives a large difference for the particle velocity (2.8 to 3.9 km/s). This would have a large effect on the von Neumann spike pressure and temperature, and hence the reaction zone profile.

An equation of state fit to HMX isothermal compression data up to pressure of 27 GPa [7, 8] is compatible with Hugoniot data, including high pressure (40 GPa) single crystal HMX data. This is the basis for a complete EOS described in [11]. The pressure is of a Mie-Grüneisen type;

$$P(V, e) = P_{\text{ref}}(V) + \frac{\Gamma(V)}{V} [e - e_{\text{ref}}(V)] ,$$

with a Birch-Murnaghan form [see for example, 12] for the reference curve. This gives a slightly curved $u_s(u_p)$ relation which is a better overall fit to the Hugoniot data. By choosing the $T = 0$ isotherm (*i.e.*, cold curve) for the reference, $e_{\text{ref}}(V) = -\int_{V_0}^V dV P_{\text{ref}}(V)$.

The temperature is determined from the specific heat;

$$e - e_{\text{ref}}(V) = \int_0^T dT' C_V(V, T') .$$

The specific heat is taken to be a function of a scaled temperature; $C_V(T, V) = \tilde{C}_V(T/\theta(V))$. Thermodynamic consistency requires that the Grüneisen coefficient is given by

$$\Gamma(V) = -\frac{d \ln \theta}{d \ln V} .$$

Thus, $\theta(V)$ plays a role analogous to a Debye temperature. The thermodynamic relation,

$$\frac{\Gamma}{V} = \frac{\beta K_S}{C_P},$$

is used to determine $\Gamma(V_0)$. Here β is the coefficient of volumetric expansion, K_S is the isentropic bulk modulus and C_P is the specific heat at constant pressure.

2.1.1 Specific heat. For a molecular crystal, the specific heat is predominantly due to lattice vibrations or phonons. The phonons can be split into two types; 3 acoustic modes and $3N - 3$ optical modes, where N is the number of atoms per molecule. For HMX ($C_4N_8O_8H_8$), $N = 28$, and there are 81 optical modes compared to 3 acoustic modes.

The acoustic modes can be described with a Debye model. Based on the sound speed, the Debye temperature for HMX is $\theta_D \sim 100$ K.¹ Consequently, above room temperature the acoustic contribution to the specific heat saturates at the classical limit of $3R/M$, where R is the gas constant [8.317 J/(mole K)], and M is the molecular weight. For HMX, $M = 0.296$ kg/mole, and the contribution to the specific heat from the acoustic modes is 0.084×10^{-3} (MJ/kg)/K. At room temperature the specific heat is about 1×10^{-3} (MJ/kg)/K. Hence, the specific heat is dominated by the optical modes.

The optical frequencies for HMX at room temperature and atmospheric pressure have been determined by infrared and Raman spectroscopy [14]. The specific heat, from the vibrational energy in the quasi-harmonic approximation, is given by

$$C_V(V, T) = \frac{R}{M} \sum_i \frac{x_i^2 \exp(x_i)}{[\exp(x_i) - 1]^2},$$

where $x_i = \theta_i(V)/T$, and $\theta_i = h\nu_i/k$ is the temperature associated with the frequency ν_i . We note that the eight highest vibrational frequency (≈ 3000 cm⁻¹ for C-H stretch) corresponds to $\theta_{\max} = 4300$ K. The temperatures associated with the other frequencies are less than 2200 K. As a consequence, at the CJ temperature of 3000 K, the specific heat is near the classical limit²; $C_V = (3N - 2)R/M = 2.3 \times 10^{-3}$ (MJ/kg)/K. The limiting value is substantially larger than published data for the specific heat [see 5, §5.3, p. 112] which extends only up to β - δ transition temperature; $C_V = 1.57 \times 10^{-3}$ (MJ/kg)/K at $T = 450$ K.³

Alternatively, the lattice vibrations and specific heat can be determined from either molecular dynamics simulations [16, see figs. 2.20, 4.13 and sec. 4.4.1] or quantum chemistry calculations [14, table 2 and fig. 2] and [15, tables 2 and 3]. The specific heat from these methods is shown in fig. 2. We note that the temperature within the reaction zone is between 2000 and 3000 K. In this regime $C_V \approx 2.0 \times 10^{-3}$ (MJ/kg)/K.

Measurements of the Raman spectrum in a diamond anvil cell show that the intra-molecular vibrational frequencies increase with compression, [see 7, fig. 8a]. The Grüneisen coefficient is the specific heat weighted average of the mode Grüneisen coefficients [see for example, 12]

$$\Gamma(V, T) = \sum_i \frac{\Gamma_i(V) \hat{C}(\theta_i(V)/T)}{\hat{C}(\theta_i(V)/T)},$$

¹The Debye temperature is given by [see for example 13, sec. 3.3] $\theta_D = \frac{h}{k} \left(\frac{3N_a}{4\pi} \right)^{1/3} \left(\frac{\rho}{ZM} \right)^{1/3} c$ where Z is the number of molecules per unit cell. With units for the sound speed c of km/s, density ρ of g/cm³ and temperature of K, $\theta_D = 251.2 \left(\frac{\rho}{ZM} \right)^{1/3} c$. For β -HMX (space group $P2_1/n$), $Z = 2$.

²At high temperatures, the four NO₂ groups become hindered rotors. This decreases the classical limit of the specific heat by $2R/M$ [see 15, p. 191].

³Experimental measurements of specific heat are at atmospheric pressure. EOS models use specific heat at constant volume. From the thermodynamic identity $C_P/C_V = K_S/K_T$, for HMX the specific heat at constant pressure is about 5% greater than at constant volume.

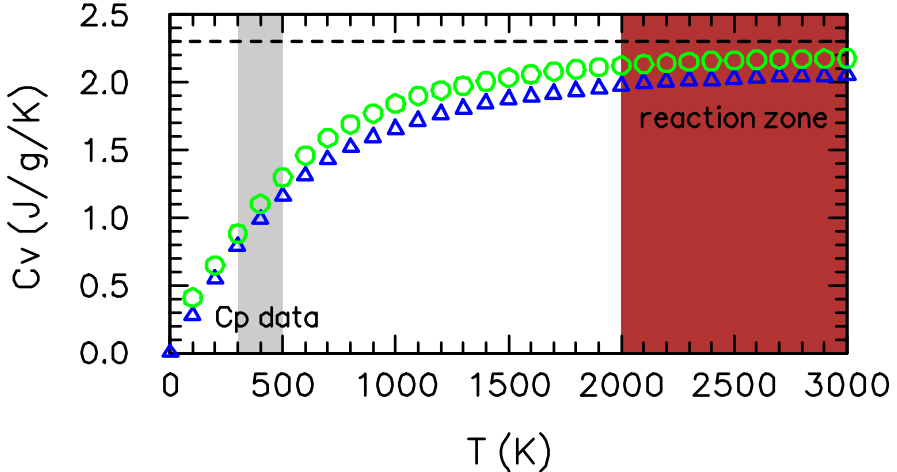


Figure 2. Specific heat for β -HMX. Blue symbols are from Goddard et al. [16, fig. 4.13], and green symbols from vibrational frequencies in Lyman et al. [15, tables 2 and 3]. C_p data (at atmospheric pressure) limited to gray region. Red area is region of interest for reaction zone. Dashed line is the classical limit.

where

$$\Gamma_i(V) = -\frac{d \ln \theta_i}{d \ln V} \quad \text{and} \quad \widehat{C}(x) = \frac{x^2 \exp(x)}{[\exp(x) - 1]^2}.$$

Since the mode Γ_i decreases as the vibrational frequency increases, the Grüneisen coefficient is in general a function of both V and T . However, the model EOS assumes that there is only one temperature scale; *i.e.*, C_V is function of $T/\theta(V)$ with the specific heat at ambient density, $C_V(T, V_0)$, fit to the calculations of Goddard et al. [16, fig. 4.13]. As a result of this simplification, the Grüneisen coefficient for the model is a function of only V .

2.2 EOS of products

For the equation of state of the reaction products a SESAME table generated by Shaw [17] is used. The products EOS is fit to data on overdriven detonations and release isentropes in PBX 9501 [18, 19]. Presently, there are no temperature data for the reaction products in the detonation regime.

The thermal part of the product EOS is based on the assumptions that the CJ temperature is 3000 K and the specific heat is 0.5 cal/g (2.07×10^{-3} (MJ/kg)/K). We note that this value of C_V is higher than the value typically associated with gaseous products. However, in the reaction zone regime, which is our main focus, the products are at high temperature and solid density. Therefore, the specific heat has contributions from vibrational modes similar to that of a solid. As the products expand, the specific heat would decrease because the translational and rotational degrees of freedom of smaller product molecules have less energy than vibrational modes.

Since our focus is on bulk burning, pressure-temperature equilibrium is appropriate for a partially burned mixture of reactants and products. This is in contrast to heterogeneous burning from hot spots, which would result in deflagration fronts separating products from reactants at different temperatures.

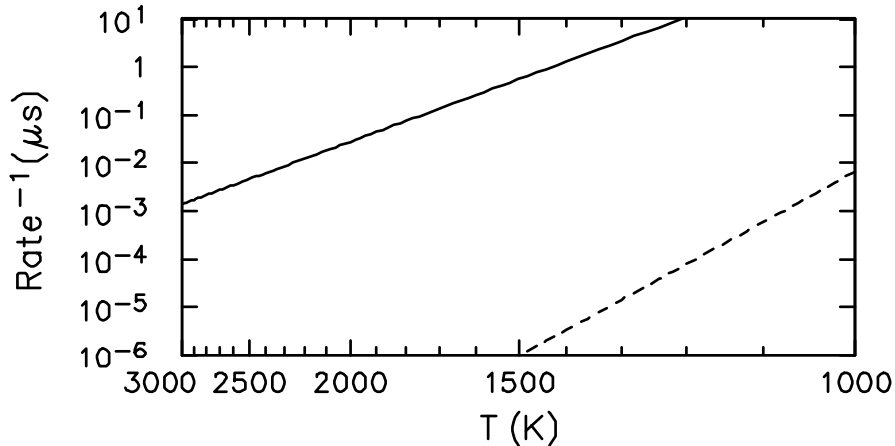


Figure 3. Inverse reaction rate vs temperature. Temperature is plotted on inverse scale. Dashed curve uses Arrhenius parameters in [5, §5.7, p. 113] ($T_a = 26522$ K, $k = 5.0 \times 10^{13} \mu\text{s}^{-1}$) and solid curve based on [20] ($T_a = 17922$ K, $k = 2.79 \times 10^5 \mu\text{s}^{-1}$).

2.3 Reaction rate

We assume a first order Arrhenius rate

$$\text{Rate}(\lambda, T) = (1 - \lambda)k \exp(-T_a/T) .$$

where λ is the reaction progress variable, and T is the temperature. For PBX 9501 we use an activation temperature $T_a = 17900$ K and multiplier $k = 2.8 \times 10^5 \mu\text{s}^{-1}$ based on the “global rate” of Henson et al. [20]. We note that the adiabatic induction time for an ideal explosive is given by

$$t_{\text{adb}} = \left[\frac{T^2 C_v}{T_a Q} \right] \frac{\exp(T_a/T)}{k} ,$$

where Q is the specific energy released by the reaction. The temperature in the ZND profile — based on the EOS of PBX 9501 — varies from 2500 K at the von Neumann spike to 3000 K at the CJ state. For HMX, $Q \sim 5$ MJ/kg, and the factor $\frac{T^2 C_v}{T_a Q} \sim 10$. The value of k has been adjusted to account for the difference between a rate needed by the simulations and the “ignition time” used in [20]. Our choice of k leads to an inverse reaction rate within the reaction zone of a few ns.

Another set of Arrhenius parameters, commonly used for simulations, is based on differential scanning calorimetry experiments of Rogers [21]; see also [5, §5.7, p. 113]. The reaction rate for these two sets of parameters is shown in fig. 3. The rates differ by several orders of magnitude.

We note that Rogers’ calorimetry experiments covered a narrow temperature range about the melting temperature of HMX; from 544 K to 558 K [21, fig. 11]. Moreover, reaction occurred on a time scale of about 30 seconds. The reaction zone time requires a very large extrapolation to the ns time scale. Due to experimental uncertainty in the measured rate, over a small temperature interval variations in T_a and k can compensate. In fact, both Henson’s and Rogers’ parameters are close to compensation line for HMX derived by Brill et al. [22, fig. 1].

The rate in the reaction zone is an enormous extrapolation from the measured regime. Rogers’ rate would give a sub ps reaction time for a CJ detonation. Since the time for a detonation wave to cross a unit cell in an HMX crystal is 0.1 ps (roughly 1 nm at 8.8 km/s = 8.8 nm/ps), Rogers’ rate is unphysically large. In contrast, Henson’s rate is compatible with the 3 high pressure data points for single crystal HMX; experiments by Craig reported in [1, p. 1065] and [23, p. 218].

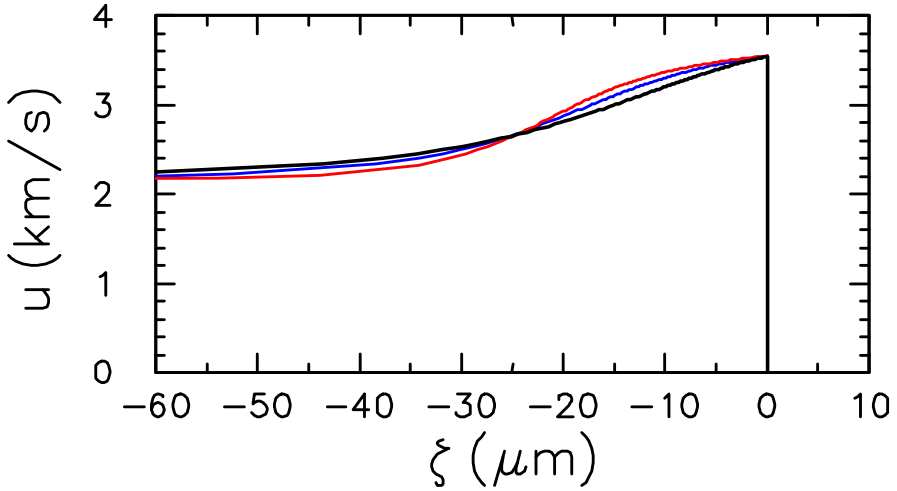


Figure 4. Particle velocity profile in the reaction zone of a steady CJ detonation wave; $\zeta = x - Dt$ is spatial coordinate. Black curve is with EOS used in simulations. Blue and red curves are for EOS with specific heat 15 and 25% higher, respectively. Arrhenius rate parameter k has been adjusted for case with higher C_V such that the curves cross at a burn fraction of $\lambda = 0.9$, which corresponds to $\zeta \approx -25 \mu\text{m}$. Velocities at von Neumann and CJ states are 3.54 and 2.17 km/s, respectively.

2.4 Model reaction zone

The steady state reaction zone profile of a detonation wave in a high explosive (HE) is determined by a system of ODEs together with the constitutive model. For PBX 9501 the particle velocity profile for a CJ wave is shown in fig. 4. Three cases are plotted to indicate the sensitivity of the profile to the specific heat. The rate has been adjusted with the specific heat such that the profiles cross at a burn fraction of $\lambda = 0.9$. We note that the reaction-zone width at 90% burnt is about $25 \mu\text{m}$, and corresponds to a reaction time of 4.3 ns. Moreover, the reaction-zone width is less than the average HMX grain size of $140 \mu\text{m}$.

For a first order reaction, the profile has a long tail. The particle velocity at 90% burn fraction, 2.67 km/s, is significantly larger than at the CJ state, 2.17 km/s, due in part to the tangency condition for the CJ state. This effect makes it difficult to determine the CJ state from the experimentally measured reaction zone profile.

The temperature at the CJ state is 3000 K. The von Neumann spike temperature is 2580 K for our standard case, and 2320 and 2140 K with the specific heat scaled 15 and 25% higher. We note that the shape of the profile is convex with the higher VN spike temperature while the other two profiles have an inflexion point. The convex case corresponds to a small temperature difference between the CJ state and VN spike state. This point is relevant to wave stability and is discussed further in a latter section.

3 Numerics

Accounting for non-linearities in the flow, equations of state, impedance match at interfaces and the reaction source term requires numerical simulations. We use the `AmTva` system of Quirk [24, 25]. The simulations are one-dimensional and use a Lagrangian second order Godunov shock capturing algorithm. In addition, adaptive mesh refinement is used to ensure that the reaction zone is fully resolved. This is needed for efficiency when the detonation wave is propagated a large distance compared to the reaction-zone width.

The Lagrangian mesh enables material interfaces to be tracked. This is convenient for VISAR simulations which include both the HE and window material. In addition, the VISAR measures the velocity time history along a particle path. This corresponds to the time history of a Lagrangian cell.

The simulations are initialized with a steady ZND wave profile. A piston boundary condition is applied with a piecewise linear velocity. A constant velocity is used for a supported wave, while a decreasing velocity is used to mock up the Taylor wave behind an unsupported self-sustaining CJ detonation wave.

3.1 Mesh refinement

The simulations use a coarse mesh with a grid spacing of $\Delta x = 2.5 \mu\text{m}$. This is roughly 10% of the reaction zone width. At least 4 levels of refinement by a factor of 2 are used. An additional level of refinement by a factor of 4 is applied at the lead shock front. This reduces the reaction within the captured shock profile, typically, to a few tenths of per cent.

Several refinement criterion are used to ensure that the reaction zone is fully resolved:

- (i) A minimum of two levels is used if $0.01 < \lambda < 0.99$.
- (ii) A level is refined if either the difference in velocity or pressure between adjacent cells is greater than 2% of the steady state VN spike value.
- (iii) There are two time constraints for numerical stability; the Courant-Friedrichs-Levy time step for hyperbolic flow, $\Delta t_{\text{CFL}} = \Delta x/c$, and the time step associated with integrating the reactive source term, $\Delta t_{\text{source}} = 1/\text{Rate}$. A level is refined if the ratio of Δt_{source} to Δt_{CFL} is greater than 1%. This is aimed at limiting the amount of burn in a cell per time step to less than 1%.

Typical, the simulations have greater than 60 cells within a half-reaction zone, *i.e.*, $0 < \lambda < 0.5$. The code has been tested on a pulsating detonation wave case studied by Sharpe and Falle [26, fig. 3], and found to be accurate.

3.2 Shock tracker

To evaluate detonation wave stability it is important to determine the time history of quantities behind the lead shock front. The shock front is determined as follows. The mesh is scanned starting from the ambient state ahead of the shock toward the reacting flow, and the quantity

$$\Delta e = e - [e_0 + \frac{1}{2}(u - u_0)^2 + P_0(V_0 - V)]$$

is evaluated. From the shock jump conditions, $\Delta e = 0$ on the Hugoniot locus. The first minimum in $|\Delta e|$ for $u - u_0$ above a noise threshold is chosen as the shock front. Front quantities are averaged over two adjacent cells. Typically, this corresponds to a small amount of reaction at the front; λ a few tenths of per cent. Due to the discretization associated with shock capturing, there is some unavoidable noise involved in picking out the shock front. The noise is of a high frequency and can be filtered out by averaging front quantities over a few times.

4 Reaction zone profile

The wave profile experiments [2, 3] used a projectile from a gas gun to initiate a planar detonation wave in PBX 9501. Two window materials were used for the VISAR; LiF (lithium fluoride)

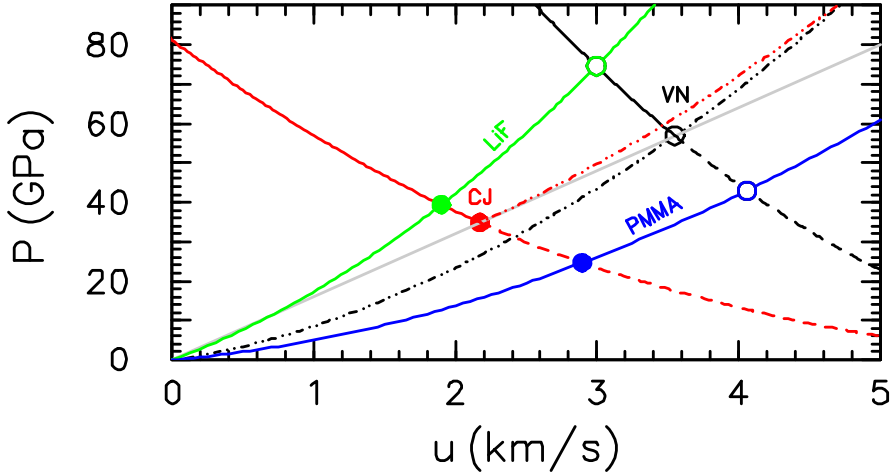


Figure 5. Impedance match for detonation wave in PBX 9501 with window. Green and blue curves are Hugoniot loci for LiF and PMMA, respectively. Black and red curves are for reactants and products, respectively. Gray is Rayleigh line corresponding to CJ detonation velocity. Labels VN and CJ denote von Neumann spike and Chapman-Jouguet state, respectively. Open circles are match from VN spike and solid circles are match from CJ state.

and PMMA (polymethylmethacrylate). We model these materials with a Hayes EOS [see 12, and references therein] fit to a linear shock velocity – particle velocity relation for the principal Hugoniot¹:

$$\begin{array}{ll} \text{LiF [10, pp. 296–297],} & \rho_0 = 2.639 \text{ g/cm}^3 \text{ and } u_s = 5.15 \text{ km/s} + 1.35 u_p; \\ \text{PMMA [10, pp. 446–451],} & \rho_0 = 1.186 \text{ g/cm}^3 \text{ and } u_s = 2.57 \text{ km/s} + 1.54 u_p. \end{array}$$

LiF has a higher impedance than HMX, while PMMA has a lower impedance. Measurements with different window materials provides a useful consistency check for interpreting the data.

Impedance matches from the VN spike and CJ state into the window are shown in fig. 5. These provide a rough check on the simulations. In addition, consistency with the expected peak velocity of the VISAR record provides a check on the EOS models and on the experimental resolution.

Interpreting the VISAR data requires understanding a few detail of the experimental setup [2]. To achieve adequate reflectivity of the laser beam, about $1 \mu\text{m}$ of aluminum is vapor deposited on the VISAR window. To ensure that the aluminum layer remains intact when impacted by the lead shock, an $8 \mu\text{m}$ thick sheet of Kapton is glued between the window and the PBX. The epoxy glue is a few μm thick. The simulations do not include these thin layers. However, their main effect can be accounted for by using as a probe point to compare with the VISAR a cell displaced from the interface on the window side. (This ignores reverberations in the aluminum layer, which have a sub ns period.) The velocity time history of cells 2.5, 10 and $25 \mu\text{m}$ from the interface are shown in fig. 6. The effect is small — a few per cent decrease in the velocity — and comparable to the accuracy of the VISAR.

The VISAR technique uses two laser beams with different fringe constants in order to determine the velocity jump across the shock front. The resolution is best when the velocity jump corresponds to an integral number of fringes. Gustavsen et al. [2, 3] estimated the VISAR time resolution at 1 to 3 ns. Because of the fringe constants used, the temporal resolution is better for with the PMMA

¹Hugoniot data for PMMA shows a jog between $3 < u_p < 4 \text{ km/s}$. This is indicative of decomposition. In addition, the reflected laser beam for the VISAR shows a decrease in intensity [see 3, fig. 2]. However, this occurs on a longer times scale than the few ns of the reaction zone. The decomposition is a non-equilibrium effect which is neglected in the EOS.

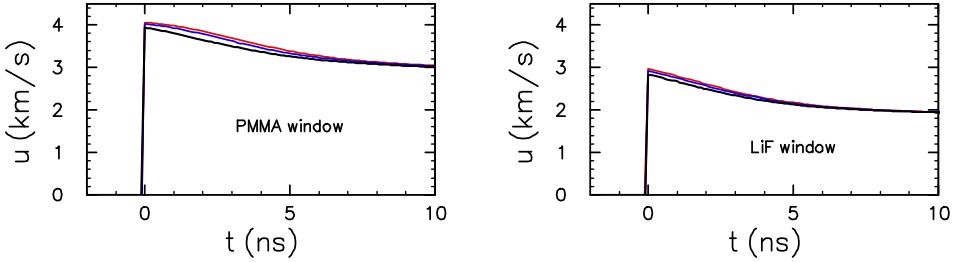


Figure 6. Effect of probe position on simulated VISAR profile. Red, blue and black curves are velocity time histories 1, 4 and 10 (coarse grid) cells from the PBX/window interface (2.5, 10 and 25 μm).

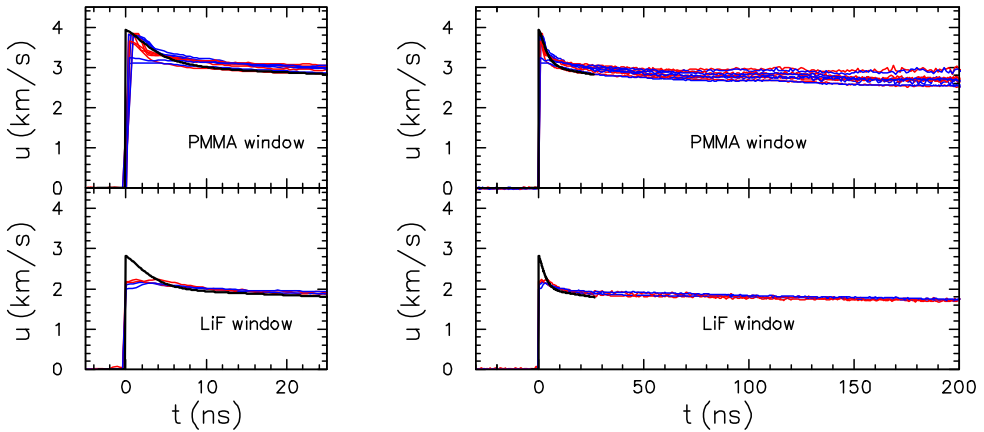


Figure 7. Comparison with VISAR data from [2, 3]. Top figures are for PMMA window and bottom are for LiF window. Left and right figures are on 25 and 200 ns time scale, respectively. Red and blue curves are experiments and black are simulations. VISAR used two laser beams with different fringe constants per experiment (red and blue). Experiments varied drive pressure for initiation and the length of PBX sample.

window than for the LiF window. For comparison, the model ZND wave profile, fig. 4, has a reaction time of about 4 ns.

Both the experimental and simulated VISAR data are shown in fig. 7. Though the VISAR record extends for about $1\ \mu\text{s}$, only the first 10 ns are relevant to the reaction zone profile. The very sharp rise of the leading edge of the profile indicates that over the VISAR laser beam the wave front is nearly flat. The laser spot size is a few hundred microns or several grains in extent. Considering the resolution, the model is compatible with the experiments using the PMMA window. For the lower resolution with the LiF window, the peak or VN spike is significantly clipped.

Our assertion, that the VN spike is clipped, is based on a related experiment by Fedorov [4]. His experiment used an explosive similar to PBX 9501. The explosive is initiated with a detonator. This gives rise to a curved detonation wave. The effect of curvature is mitigated by using a large charge. The velocity time history at a LiF window is measured using a Fabry-Perot interferometry technique with 1 ns time resolution. The measurement [4, fig. 2a] clearly displays a ZND reaction zone profile. The VN peak is slightly lower and the temporal width is wider than the model profile, fig. 4. This is compatible with a curved detonation front (or possibly slightly lower HMX weight fraction) having a slightly lower detonation velocity. We also note that the shape of the experimental profile is convex. This corresponds to the EOS with the higher VN spike temperature; black curve in fig. 4.

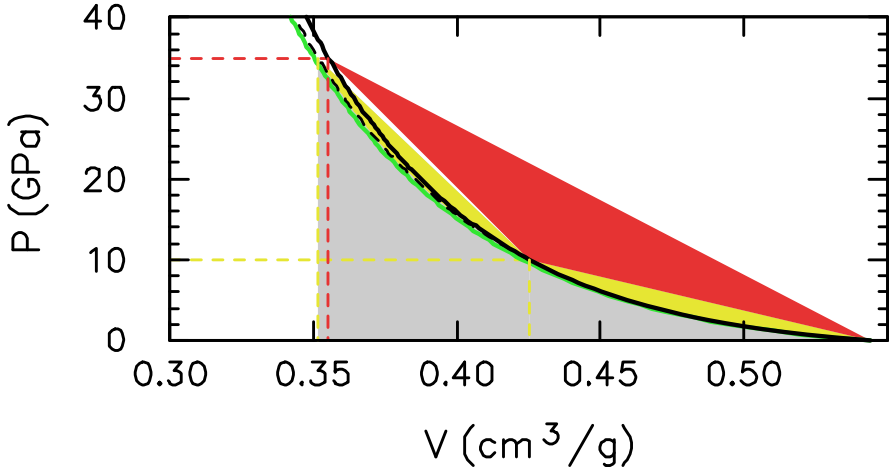


Figure 8. Graphical representation of shock heating. Solid and dashed black curves are Hugoniot loci from initial state and first shock at 10 GPa. Green curve is isotherm through the initial state. Gray region corresponds to energy from isentropic compression. Heating for double shock corresponds to yellow regions, while single shock corresponds to yellow plus red regions.

5 Shock desensitization

Experiments have shown that a weak shock can desensitize a PBX to the point of quenching a propagating detonation wave[1]. This appears to be at odds with an under driven or CJ detonation wave sustained by the reaction rate from the bulk shock temperature. The key to reconciling these properties is the dependence of the shock temperature on the initial density.

The jump in the specific internal energy across a shock is given by $\Delta e = \frac{1}{2}(P + P_0)(V_0 - V)$. In the (V, P) -plane, the energy change is the area of trapezoid. This can be split into the energy from isentropic compression and shock heating. The temperature for isentropic compression is given by $T_s = T_0 \exp[\Gamma(V_0 - V)/V_0]$. For PBX 9501, the temperature increases by about 170 K at the compression of the VN spike. The bulk of the temperature rise across a shock comes from shock heating; $\Delta T = (\text{dissipative energy})/Cv$.

Solids are stiff materials. The bulk modulus of PBX 9501 is 9.4 GPa at the initial state and increases to 280 GPa at the von Neumann spike. Since the modulus is large, shocks up to the von Neumann spike pressure are weak in terms of the entropy change. Consequently, the Hugoniot locus and the isentrope are nearly the same. This enables a decomposition of the Hugoniot energy as follows. The isentropic energy is approximately the area under the Hugoniot locus, while shock heating is approximately the area between the Rayleigh line and the Hugoniot locus. The effect of a single shock compared to a double shock is illustrated in fig. 8. Because of the convexity of the Hugoniot locus, the dissipative energy is much larger for a single shock than for a double shock. The geometric interpretation implies that this is a generic property of shocks.

As an example we consider the precompression from a 2 GPa shock. The quantitative effect on temperature is shown in fig. 9. In addition, the CJ and VN pressures are marked. It is noteworthy that the double shock temperature is significantly lower than a single shock to the same pressure.

The temperature variation greatly affects the reaction rate. Important quantities at the CJ state and VN spike are listed in table 1. We note that the detonation speed in the precompressed PBX is slightly higher since the chemical energy density is higher. But the temperature is lower because shock heating is lowered by the precompression. Due to the temperature sensitivity, the reaction rate changes by a factor 3. Consequently, the reaction zone width is larger in the precompressed than in the pristine PBX.

Of importance for understanding shock desensitization are the impedance matches from the CJ state and VN spike of the propagating detonation wave into the precompressed PBX. These are

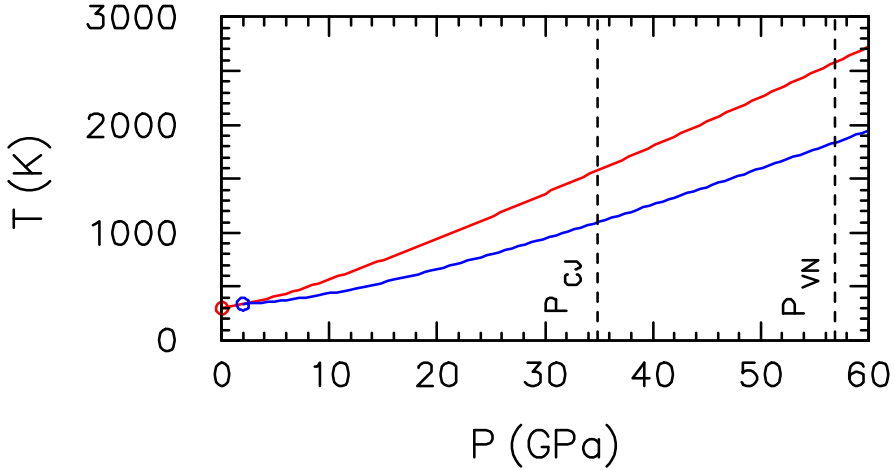


Figure 9. Shock temperature for PBX 9501. Red curve is shock locus from the initial state. Blue curve is locus from precompressed state of a 2 GPa shock. Dashed line denote the pressure at the CJ state and VN spike.

Table 1. End states of detonation wave in ambient and precompressed PBX 9501.

	ambient	(2 GPa) compressed	
ρ_0	1.83	2.03	g/cm ³
u_s	8.8	9.4	km/s
VN spike			
ρ	3.07	3.19	g/cm ³
P	56.9	67.7	GPa
T	2580.	2230.	K
Rate ⁻¹	3.7	11.2	ns
CJ state			
ρ	2.43	2.67	g/cm ³
P	34.8	45.2	GPa
T	3000.	2640.	K

listed in table 2. Two observations are critical to shock desensitization. First, the impedance match from the CJ state gives rise to a relatively low temperature, 1100 K, in the precompressed PBX. Consequently, the induction time for reaction is very long. This is consistent with experiment by Campbell and Travis [1, p. 1062] in which a detonation wave in PBX 9404 (approximately the same CJ pressure as for PBX 9501) did not initiate a large 13 mm single crystal of HMX. Second, even the impedance match from the higher pressure of the VN spike results in the precompressed PBX having a temperature several hundred degrees lower than the temperature behind the incident VN spike state. Consequently, the reaction time in the precompressed material is significantly larger than that within the reaction zone of the incident detonation wave.

The impact of a detonation wave on the precompressed PBX can be viewed as an initiation problem with a high pressure short duration pulse, *i.e.*, from pressure profile in the reaction zone of incident detonation wave. Since the pulse is shorter than that of the reaction zone of the precompressed PBX, one can expect the following sequence of events:

Table 2. Results in precompressed PBX 9501 following impedance matches from states of ambient detonation wave.

	VN spike	CJ state	
P	64.2	35.0	GPa
T	2100.	1100.	K
Rate ⁻¹	18.5	41500.	ns

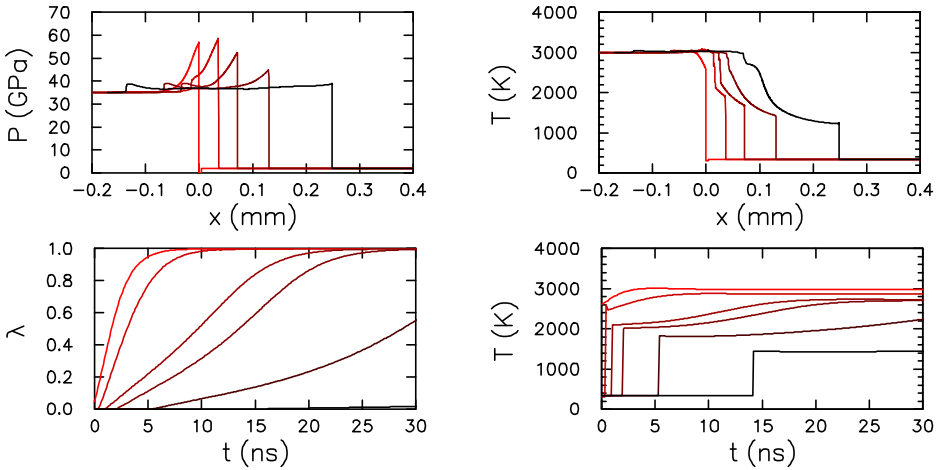


Figure 10. Evolution of detonation wave into PBX precompressed by 2 GPa shock. On top are spatial profiles at $t = 0, 4, 8, 15, 30$ ns. Bottom plots are Lagrangian time histories at $x = 0, 5, 10, 20, 50, 125 \mu\text{m}$.

- (i) Impedance match with VN spike lowers the temperature and hence the reaction rate behind the lead shock.
- (ii) Without sufficient support from reaction, lead shock decays. Hence, the temperature and reaction rate further decrease.
- (iii) The feedback continues until the limiting case is reached corresponding to the impedance match from CJ state of detonation wave into precompressed PBX.

Moreover, the transient over which the detonation wave quenches occurs on a fast time scale because of the sensitive dependence of the rate on the temperature. The transient time scale is on the order of the reaction time within the steady reaction zone.

Simulations of a detonation wave impinging on precompressed PBX bear out this sequence of events. The time evolution of the wave are shown in fig. 10. The decay of the lead shock is clearly seen in the spatial profile. The Lagrangian time histories show the induction time for the reaction increasing as the lead shock decays. At the end of the simulation, the lead wave in the precompressed PBX is approaching the result of the impedance match from the CJ state of the incident detonation wave.

On the sub μs time scale of the simulation, the detonation wave appears to fail. If the simulation were continued, the temperature behind the lead shock would re-initiate the detonation wave after a long induction time. In other words, the solution would be a galloping detonation wave; pulsating with a long period. Physically, however, with hot products adjacent to reactants, heat conduction would result in a transition to a deflagration wave. At CJ pressure, the deflagration velocity is $\sim 1 \text{ km/s}$ [27]. Thus, even when a detonation wave fails on the μs time scale of a desensitization experiment, the HE would burn on a ms time scale. Therefore, one would not expect to recover any unburnt HE, except for the edges of a charge that were quenched by strong rarefactions from the

side boundaries.

The coefficient of thermal diffusion for HMX is $\kappa \sim 1\mu\text{m}^2/\mu\text{s}$. For a propagating detonation wave, the reaction time is $\Delta t \sim 4\text{ ns}$, and thermal diffusion has a small spatial extent of $(\kappa\Delta t)^{1/2} \sim 0.06\mu\text{m}$. This is much less than the reaction-zone width of $\sim 25\mu\text{m}$. Hence, thermal diffusion would have a negligible effect on the profile of a steady detonation wave. It is not included in the simulations.

We remark that engineering simulations typically use burn models with pressure dependent reaction rates. Burn models are intended to account for subgrid effects that are not resolved. Pressure dependent rate models can only account for shock desensitization with a switch on the reaction rate. The switch is sometimes based on the pressure of the lead shock. Heuristically, this mocks up the effect on the reaction rate due to changes in the hot-spot distribution. Qualitatively, these models can describe shock desensitization. However, for PBX 9501 the underlying physics is not correct, and when applied to shock desensitization would be quantitatively inaccurate. We also note that mesoscale initiation simulations, in which hot spots are fully resolved, need to use a chemical reaction rate. Chemical rates, such as used here, are typically temperature dependent.

6 Stability

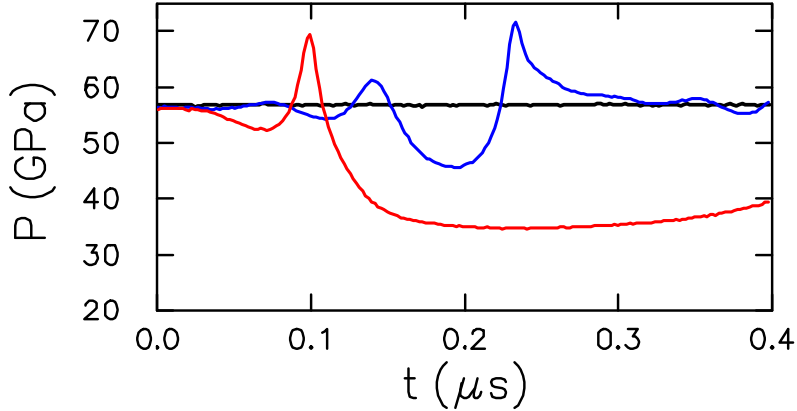
An Arrhenius rate with a high activation temperature is very temperature sensitive. This played a critical role in the analysis of shock desensitization in the previous section. Temperature sensitive rates are also associated with detonation wave instabilities. In one dimension, the instability is manifest as a pulsation or galloping detonation [see for example 6, chpt. 6A]. In addition to activation temperature, the effective temperature sensitivity depends on the variation of the temperature within the reaction zone.

For a steady detonation wave, the reaction zone temperature $T(\lambda)$ depends only on the equation of state, *i.e.*, it is independent of the rate. The temperature variation depends largely on the CJ state temperature of the products and the VN spike temperature of the reactants. In contrast to model explosives with an ideal gas EOS, for which stability has been extensively analyzed, with separate equations of state for the reactants and products, the CJ and VN temperatures are independent. For our PBX 9501 model, the specific heat of the reactants is scaled in order to vary the VN spike temperature. With the standard model, the VN spike temperature is only slightly lower than the CJ state temperature. Increasing the specific heat lowers the VN spike temperature and increases the temperature variation within the reaction zone.

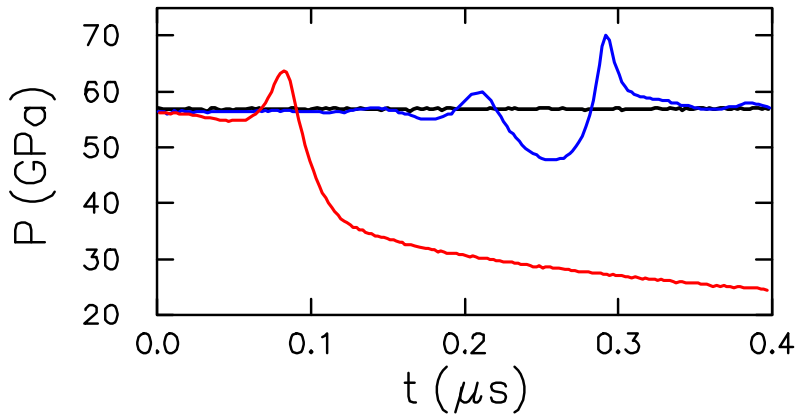
To show the effect on detonation wave stability, simulations are run in which a detonation wave is propagated over a large distance (3.5 mm) compared to the half reaction-zone width ($9.7\mu\text{m}$) of a steady wave. The simulations used a piston boundary condition. A piston velocity set at the CJ particle velocity is used for a supported detonation, while a decreasing piston velocity is used for an unsupported detonation. In applications, CJ detonation waves are self-sustaining. Thus, the unsupported boundary condition is more realistic.

A good measure of detonation stability is the pressure at the lead shock front. The results of the simulations are shown in fig. 11. There is a marked effect with the temperature variation in the reaction zone. With a small temperature variation the detonation wave is stable. For a large temperature variation, the detonation wave appears to fail, though the supported wave would reinitiate after an induction time. At the end of the simulation, the wave profile for this case is similar to that of the quenched detonation wave in the previous section. The intermediate temperature variation shows an oscillation and corresponds to a galloping detonation wave. On the low amplitude side of the oscillation, the end of the reaction zone is subsonic with respect to the front. Thus, if the oscillation grow sufficiently large, one would expect the unsupported wave to fail.

The simulations only describe a homogeneous explosive. Physically, when bulk burn is not sufficient to support a stable detonation, hot spots in a PBX would become important for propagating the detonation wave. A similar effect occurs for gaseous detonations. A two-dimensional instability is manifest by transverse waves propagating within the reaction zone. Hot spots result from the collision of the transverse waves. Analogous to the desensitization experiments in the previous section, the gaseous hot spots can be suppressed by absorbing the transverse waves along the side boundaries. Experiments [28] have shown that, for some gaseous explosives, suppressing the transverse waves can quench a propagating detonation wave.



A. Supported



B. Unsupported

Figure 11. Time history of shock pressure for CJ detonation wave: A. supported; B. unsupported. Black curve is with EOS used in simulations of VISAR experiment. Blue and red curves are for EOS with specific heat scaled 15 and 25 % higher.

For PBX 9501, two other points are worth noting. (i) In addition to affect on stability, the specific heat of the reactants also affects the shape of the reaction zone profile. For the model EOS, the stable velocity profile is convex, black curve in fig. 4, and corresponds to the shape of the profile measured by Fedorov [4, fig. 2a]. (ii) The shape of the detonation front is measured in rate stick experiments used to determine the curvature effect — $D(\kappa)$ relation needed for the detonation-shock-dynamics model. For PBX 9501, the detonation front is very smooth Hill [29]. This indicates that the detonation wave is stable, even in three-dimensions. Multi-dimensional stability simulations of PBX 9501 have not yet been performed.

7 Discussion

For PBX 9501 we have shown that the planar reaction zone profile, shock desensitization and detonation stability are all compatible with a reaction rate based on the bulk temperature. This perspective is consistent with other experiments. Two related phenomena merit further discussion: (i) Failure

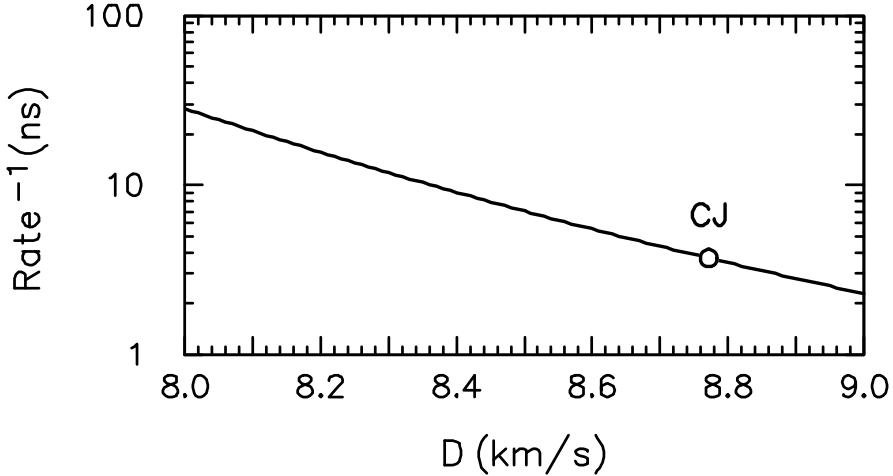


Figure 12. Inverse reaction rate behind lead shock as function of shock speed. Circle marks planar CJ detonation speed.

diameter which does depend on heterogeneities in a PBX. (ii) PBXs with lower HMX content which display irregular detonation fronts. Both effects are due to a change in burn mode; from bulk burn to hot spot dominated burn as described below.

7.1 Failure diameter

The curvature of a detonation front lowers the detonation speed. This in turn lowers the temperature behind the lead shock of the reaction zone, and hence the bulk reaction rate. For PBX 9501, the reaction time (inverse rate) as a function of detonation speed is shown in fig. 12. Due to the Arrhenius rate, the reaction time varies exponentially with the detonation speed. A ten per cent decrease in the detonation speed increases the time by a factor of 10. This would increase the reaction zone width to be greater than the average HMX grain size of $140\ \mu\text{m}$. One would expect that hot spots occur on the length scale of heterogeneities set by the grain size. Moreover, if the reaction-zone width from bulk burning exceeds the hot-spot length scale, then burning would be dominated by the hot spots.

For a steady detonation wave propagating in a rate stick, the front curvature increases from the center to the edges. Typically, for a heterogeneous explosive, the detonation speed at the failure diameter is about 10 % less than the planar detonation speed [30]. This suggests that as the diameter of a rate stick decreases, there will be a change in reaction mode; from homogeneous or bulk reaction at the center to heterogeneous or hot spot dominated burn along the edges. As a consequence, the failure diameter, which results from a rarefaction propagating inward from the edges, does depend on hot spots and hence the formulation of a PBX (grain distribution and binder).

The hypothesis of a change in burn mode could be tested by measuring the variation of the reaction zone profile across the diameter of a rate stick near the failure diameter of the explosive. The recent development of line VISARs makes such an experiment feasible. However, to observe the change in reaction mode, one would need 1 ns temporal resolution and subgrain spacial resolution, say 20 or $30\ \mu\text{m}$, with a spatial extent of several grains, say 1 mm.

Other researchers have proposed a change in reaction mechanism; see for example, Dremin and Shvedov [31], Klimentko [32]. The change in burn mode was motivated by experiments with granular explosives in which pores are filled with different gases or liquids. It is observed that the reaction time becomes independent of the fill at roughly half of the CJ pressure; 15 GPa for RDX (cyclo-trimethylene-trinitramine) which is similar to HMX. This led to the hypothesis that a change in reaction mechanism is triggered by pressure.

Granular explosives are similar to PBXs with low HE content. As described in the next subsection, the reaction zone for this type of explosive is dominated by hot spots. Consequently, the change in the dependence of reaction time at half the CJ pressure must be due to a change in the dissipative mechanism for generating hot spots; for example, from pore collapse with viscous heating to micro-jetting within the pore. In contrast, the hypothesis here is that homogeneous reaction from the bulk shock temperature dominates when it results in a reaction-zone length less than the scale of the heterogeneities.

7.2 *Low HMX content PBX*

The chemical energy density of a PBX is proportional to its HE content. As a consequence, the detonation speed decreases as the the weight per cent of binder increases. This affects the temperature behind the lead shock and hence the reaction rate. As with the curvature effect, there is a change in reaction mode when the detonation speed is sufficiently lowered. Thus, the HE content in a PBX can have a qualitative effect on the reaction zone of a detonation wave.

This effect is illustrated by experiments of Plaksin et al. [33]. They used a PBX with an HMX mass fraction of 80%. The measured detonation speed of 8.0 km/s is similar to that of PBX 9501 at its failure diameter. The observed detonation front had an irregular structure indicative of a hot spot dominated reaction zone. This is in contrast to PBX 9501 with an HMX mass fraction of 95%, which has a smooth detonation front sustained by the reaction from the bulk temperature.

Experiments of Loboiko and Lubyatinsky [34], Lubyatinsky and Loboiko [35] are also noteworthy. They observed different reaction zone structures for different PBXs with a wide range of HE content. However, for very high HE content, with only 5 ns resolution, the VN spike is not observed. In effect, the VN spike is seen on spatially averaged profile of pressed PBXs when hot spot dominated reaction zone width is sufficiently long to be resolved. This points out the need for at least 1 ns temporal resolution for reaction zone experiments. Furthermore, in order to interpret the results for hot spot dominated reaction zones one needs to be cognizant of the spatial averaging of the measurement compared to the length scale of the hot spots.

7.3 *Final remarks*

Simulations require constitutive properties as input. Some results, such as the stability of a detonation wave, are sensitive to material parameters. EOS data in the reaction zone regime is very limited.

In particular, for PBX 9501, there is no data on the temperature of the products near the CJ state. The reactant Hugoniot at the VN state is an extrapolation from low pressure data. We note that fig. 5 shows the reactant Hugoniot crosses the detonation locus at about 90 GPa. Though unexpected this does not violate any physical principal. It may indicate that HMX decomposes under pressure. Or it may be an inaccuracy resulting from the assumed fitting form of the reactant EOS. In addition, the reaction rate is based on measurements at temperatures well below the estimated 3000 K CJ temperature.

The conclusion that bulk burn dominates the reaction for a planar detonation wave is consistent with data on the reaction zone profile. It is also compatible with data on a range of other detonation phenomena.

Acknowledgments

This work was carried out under the auspices of the U. S. Dept. of Energy at LANL under contract W-7405-ENG-36. The author thanks Rick Gustavsen for providing VISAR data files from the detonation wave profile experiments, and James Quirk for creating the Am^qt^a environment used for the simulations presented here and for his generous aid in teaching how to use it effectively.

References

- [1] A. W. Campbell and J. R. Travis. The shock desensitization of PBX-9404 and composition B-3. In *Eighth Symposium (International) on Detonation*, pages 1057–1068, 1986.
- [2] R. L. Gustavsen, S. A. Sheffield, and R. R. Alcon. Detonation wave profiles in HMX based explosives. In *Shock Compression of Condensed Matter – 1997*, pages 739–742, 1998.
- [3] R. L. Gustavsen, S. A. Sheffield, and R. R. Alcon. Progress in measuring detonation wave profiles in PBX9501. In *Eleventh (International) Symposium on Detonation*, 1998.
- [4] A. V. Fedorov. Detonation wave structure in liquid homogeneous, solid heterogeneous and agatized HE. In *Twelfth (International) Symposium on Detonation*, 2002.
- [5] T. R. Gibbs and A. Popolato, editors. *LASL Explosive Property Data*. Univ. of Calif. Press, 1980.
- [6] W. Fickett and W. C. Davis. *Detonation*. Univ. of Calif. Press, 1979.
- [7] C.-S. Yoo and H. Cynn. Equation of state, phase transition, decomposition of β -HMX. *J. Chem. Phys.*, 111:10229–10235, 1999.
- [8] R. Menikoff and T. D. Sewell. Fitting forms for isothermal data. *High Pressure Research*, 21: 121–138, 2001.
- [9] S. A. Sheffield, R. L. Gustavsen, R. R. Alcon, D. L. Robbins, and D. B. Stahl. High pressure hugoniot and reaction rate measurements in PBX 9501. In *Shock Compression of Condensed Matter – 2003*, pages 1033–1036, 2004.
- [10] S. P. Marsh, editor. *LASL Shock Hugoniot Data*. Univ. of Calif. Press, 1980.
- [11] R. Menikoff and T. D. Sewell. Complete equation of state for beta-HMX and implications for initiation. In *Shock Compression of Condensed Matter – 2003*, pages 157–160, 2004.
- [12] R. Menikoff. Empirical equations of state for solids. In Y. Horie, editor, *Shock Wave Encyclopedia: Shock Waves in Solids*. Springer-Verlag, in preparation.
- [13] Jean-Paul Poirier. *Introduction to the Physics of the Earth's Interior*. Cambridge Univ. Press, 1991.
- [14] H. V. Brand, R. L. Rabie, D. J. Funk, I. Diaz-Acosta, P. Pulay, and T. K. Lippert. Theoretical and experimental study of the vibrational spectra of the α , β , and δ phases of octahydro-1,3,5,7-tetranitro-1,3,5,7-tetrazocine (HMX). *J. Phys. Chem. B*, 106:10594–10604, 2002.
- [15] J. L. Lyman, Y.-C. Liau, and H. V. Brand. Thermochemical functions for gas-phase, 1,3,5,7-tetranitro-1,3,5,7-tetraazacyclooctane (HMX), and its larger reaction products. *Combust. Flame*, 130:185–203, 2002.
- [16] W. A. Goddard, D. I. Meiron, M. Ortiz, J. E. Shepherd, and J. Pool. Annual technical report. Technical Report 032, Center for Simulation of Dynamic Response in Materials, Calif. Inst. of Tech., 1998.
<http://www.cacr.caltech.edu/ASAP/publications/cit-ascii-tr/cit-ascii-tr032.pdf>.
- [17] M. S. Shaw, 2004. private communication.
- [18] R. S. Hixson, M. S. Shaw, J. N. Fritz, J. N. Vorthman, and W. W. Anderson. Release isentropes of overdriven plastic-bonded explosive PBX 9501. *J. Appl. Phys.*, 88:6287–6293, 2000.
- [19] J. N. Fritz, R. S. Hixson, M. S. Shaw, C. E. Morris, and R. G. McQueen. Overdriven-detonation and sound-speed measurements in PBX 9501 and the thermodynamic Chapman-Jouguet pressure. *J. Appl. Phys.*, 80:6129–6149, 1996.
- [20] B. F. Henson, B. W. Asay, L. B. Smilowitz, and P. M. Dickson. Ignition chemistry in HMX from thermal explosion to detonation. In *Shock Compression of Condensed Matter – 2001*, pages 1069–1072, 2002.
- [21] R. N. Rogers. Differential scanning calorimetric determination of kinetics constants of systems that melt with decomposition. *Thermochimica Acta*, 3:437–447, 1972.
- [22] T. B. Brill, P. E. Gongwer, and G. K. Williams. Thermal decomposition of energetic materials: Kinetic compensation effects in HMX, RDX and NTO. *J. Phys. Chem.*, 98:12242–12247, 1994.
- [23] C. L. Mader. *Numerical Modeling of Explosives and Propellants*. CRC Press, second edition, 1998.
- [24] J. J. Quirk. Amrita - a computational facility for CFD modelling. In *29th Computational Fluid Dynamics*, VKI Lecture Series, chapter 4. von Karmen Institute, 1998. URL http://www.amrita-ebook.org/pdf/vki/cfd29/jjq/vki:cfd29::jjq_11.pdf.
- [25] J. J. Quirk. AMR_sol: Design principles and practice. In *29th Computational Fluid Dynamics*, VKI Lecture Series, chapter 5. von Karmen Institute, 1998. URL http://www.amrita-ebook.org/pdf/vki/cfd29/jjq/vki:cfd29::jjq_12.pdf.

- [26] G. J. Sharpe and S. A. E. G. Falle. Numerical simulations of pulsating detonations: I. nonlinear stability of steady detonations. *Combust. Theory Modelling*, 4:557–574, 2000.
- [27] A. P. Esposito, D. L. Farber, J. E. Reaugh, and J. M. Zaug. Reaction propagation rates in HMX at high pressure. *Propellants, Explosives, Pyrotechnics*, 28:83–88, 2003.
- [28] M. I. Radulescu and J. H. S. Lee. The failure mechanism of gaseous detonations: Experiments in porous wall tubes. *Combust. Flame*, 131:29–46, 2002.
- [29] L. G. Hill. DSD calibration of PBX 9501 and PBX 9404. Technical Report LA-UR-01-6127, Los Alamos National Laboratory, 2001. Slides for presentation at LANL HE review meeting Jan. 2002.
- [30] A. W. Campbell and R. Engelke. The diameter effect in high-density heterogeneous explosives. In *Sixth (International) Symposium on Detonation*, pages 642–652, 1976.
- [31] A. N. Dremin and K. K. Shvedov. On shock wave explosive decomposition. In *Sixth Symposium (International) on Detonation*, pages 29–35, 1976.
- [32] V. Y. Klimenko. Homogeneous mechanisms for detonation of heterogeneous HE. In *Shock Compression of Condensed Matter – 2003*, pages 355–358, 2004.
- [33] I. Plaksin, J. Campos, P. Simões, A. Portugal, J. Ribeiro, R. Mendes, and J. Góis. Detonation study of energetic micro-samples. In *Twelve Symposium (International) on Detonation*, 2002. URL <http://www.intdetsymp.org/detsymp2002/PaperSubmit/FinalManuscript/pdf/Plaksin-094.PDF>.
- [34] B. G. Loboiko and S. N. Lubyatinsky. Reaction zones of detonating solid explosives. *Combustion Explosion and Shock Waves*, 36:716–733, 2000.
- [35] S. N. Lubyatinsky and B. G. Loboiko. Density effect on detonation reaction zone length in solid explosives. In *Shock Compression of Condensed Matter – 1997*, pages 743–746, 1998.